JTTEE5 23:1445–1455
DOI: 10.1007/s11666-014-0134-x
1059-9630/$19.00 © ASM International

Tin-Incorporation Induced Changes in the Microstructural, Optical, and Electrical Behavior of Tungsten Oxide Nanocrystalline Thin Films Grown Via Spray Pyrolysis

Ramnayan Mukherjee, C.S. Prajapati, and P.P. Sahay

(Submitted May 8, 2014; in revised form July 2, 2014)

Undoped and Sn-doped WO_3 thin films were grown on cleaned glass substrates by chemical spray pyrolysis, using ammonium tungstate $(NH_4)_2WO_4$ as the host precursor and tin chloride $(SnCl_4{\cdot}5H_2O)$ as the source of dopant. The XRD spectra confirm the monoclinic structure with a sharp narrow peak along (200) direction along with other peaks of low relative intensities for all the samples. On Sn doping, the films exhibit reduced crystallinity relative to the undoped film. The standard deviation for relative peak intensity with dopant concentration shows enhancement in heterogeneous nucleation growth. As evident from SEM images, on Sn doping, appearance of island-like structure (i.e., cluster of primary crystallites at few places) takes place. The transmittance has been found to decrease in all the Sn-doped films. The optical band gap has been calculated for both direct and indirect transitions. On Sn doping, the direct band gap shows a red shift and becomes 2.89 eV at 2 at.% doping. Two distinct peaks, one blue emission at 408 nm and other green emission at 533 nm, have been found in the PL spectra. Electrical conductivity has been found to increase with Sn doping.

Keywords electrical properties, Sn-doped WO_3 thin films, spray pyrolysis, structural and optical properties

1. Introduction

The prospective use of semiconductor metal oxide nanostructures in present and future technological field is highly attractive due to their excellent optical and electronic properties. Tungsten oxide (WO_3) is among a few of them, which is expected to play an important role in future technology due to its outstanding electrochromic (Ref 1), thermochromic (Ref 2), photochromic (Ref 3), gaschromic (Ref 4), gas sensor (Ref 5), fuel cell (Ref 6), super-hydrophilic (Ref 7, 8), photocatalytic (Ref 9), and photoluminescence properties (Ref 10). WO_3 has been extensively used in large scale as a photoanode for photoelectrochemical water-splitting systems since the mid-1970s. It can easily be grown in thin film form with high optical transparency within the visible region and good transport properties. WO_3 thin films have already been used to prepare newly invented gadgets and devices like smart-window, anti-dazzling rear view mirrors for cars, eye wear, electronic nose, non-emissive displays, and solid state gas and temperature sensors (Ref 11-14).

WO_3 is an n-type wide band gap (2.6-3.6 eV) semiconductor (Ref 13). Various techniques have been used to fabricate WO_3 thin films which include vacuum evaporation (Ref 15), pulse laser deposition (Ref 16), RF sputtering (Ref 17), electron beam evaporation (Ref 18), anodic oxidation (Ref 19), sol-gel (Ref 20), hydrothermal (Ref 21), spray pyrolysis (Ref 11), and so forth. Here, we have used chemical spray pyrolysis technique for our film growth as it is a simple and straightforward technique that does not require complicated and expensive instrumentations and is ideal for large area coating. Spray pyrolysis also provides good reproducibility in terms of thickness, crystallinity, and stoichiometry for the thin films.

To develop successful semiconducting technology for the future and to cope with the increasing demand for new devices, emphasis must be given to the characterizations and measurement of various physical parameters of semiconducting materials. One of the important tools to tailor the characteristics and to get the desired properties of the films is the inlay of dopants into the parent system. For practical applications, various dopants such as Li (Ref 22), Fe (Ref 18), Al (Ref 23), Au (Ref 24), Ti (Ref 25), and Nb (Ref 26) have been used to improve the desired characteristics of WO_3 materials. The structure, surface morphology, optical, and electrical properties of WO_3 films are very important for electrochromic, gas sensor, and catalytic applications. To the best of our knowledge, the effect of Sn doping on the structural, optical, and electrical properties of spray-deposited Sn-doped WO_3

Ramnayan Mukherjee and **P.P. Sahay**, Department of Physics, Motilal Nehru National Institute of Technology, Allahabad 211 004, India; and **C.S. Prajapati**, Center for Nano Science and Engineering, Indian Institute of Science, Bangalore 560012, India. Contact e-mail: dr_ppsahay@rediffmail.com.

thin films has not yet been reported in the literature. Keeping these in view, a detailed study of the structural, morphological, optical, and electrical properties of Sn-doped WO_3 thin films have been carried out and presented in this paper.

2. Experimental

2.1 Preparation of WO_3 Thin Film

Undoped WO_3 thin films were prepared using the precursor solution of ammonium tungstate $(NH_4)_2WO_4$. The precursor solution was prepared by dissolving $(NH_4)_2WO_4$ in hot deionized water (60-65 °C). For Sn-doped films, tin chloride ($SnCl_4{\cdot}5H_2O$) was taken as the source of dopant. Dopant concentration (Sn/W ratio) was varied from 0 to 2 atomic percent (at.%). The solution concentration was optimized after several depositions and was fixed at 0.1 M throughout this work. The atomization of the solution into a spray of fine droplets was carried out by a glass nozzle, with the help of compressed air as the carrier gas. Details of the spray system and other process parameter have been described elsewhere (Ref 27). The solution was sprayed onto the ultrasonically cleaned, preheated micro glass substrates. During the course of spraying, the substrate was kept at a constant temperature of 400 ± 10 °C. $(NH_4)_2WO_4$ decomposed pyrolytically into WO_3 at this temperature and got deposited onto micro glass substrates, according to the following endothermic reaction (Ref 13, 28):

$$(NH_4)_2WO_4 \rightarrow WO_3 + 2NH_3 + H_2O$$

The thickness of the deposited films was measured using gravimetric weight difference method and found to be in the range of 500-550 nm. The film thickness was also estimated from the cross-sectional SEM view of the film, and the results were in good agreement to those measured using gravimetric weight difference method.

2.2 Characterizations

Both undoped and doped WO_3 thin films were characterized using different techniques. The structure of deposited films has been confirmed by x-ray diffraction analyses using a Bruker AXS C-8 advanced diffractometer with CuKα radiation (λ = 1.5406 Å) as an x-ray source. Surface image analyses of the films were carried out using a JEOL scanning electron microscope (SEM) and a NTEGRA atomic force microscope (AFM). Compositional analysis of the films was done through energy-dispersive x-ray spectroscopy (EDX) attached to SEM. The optical properties of the films were studied using Perkin Elmer Lambda 35 UV-Vis spectrometer (UK) in the spectral range 300-800 nm. The measurements were performed in the wavelength scanning mode with the beam being in the normal incidence setup. The photoluminescence (PL) spectra were carried out with VARIAN CARY eclipse fluorescence spectrophotometer. The excitation source was a Xenon-lamp (290 nm), and the sample temperature was kept at room temperature. The temperature dependence of the electrical conductivity of the films was studied using an indigenously designed experimental setup equipped with Keithley System Electrometer (Model: 6517B). High conducting colloidal silver was used to make ohmic contacts on both ends of the films for electrical measurements.

3. Results and Discussion

In spray pyrolysis technique, when the fine droplets of precursor solution arrive close to the heated substrate, the reactant molecules undergo chemical decomposition which leads to nucleation, crystal growth, and finally film formation. The films thus prepared are now undertaken for further characterizations.

3.1 Structural Characterization

3.1.1 XRD Analyses. Figure 1 shows x-ray diffraction patterns of the films with various Sn concentrations. All the reflection peaks have been indexed with the pure monoclinic WO_3 with lattice constants $a = 7.297$ Å, $b = 7.539$ Å, $c = 7.688$ Å, and $\beta = 90.91°$ (JCPDS card no. 24-0747). No other phase corresponding to Sn or other compound has been found in the XRD spectra. Similar XRD results were reported by Yoon et al. (Ref 29). The diffractogram shows a narrow peak with the highest intensity along (200) direction for all the samples, which indicates that the film has favorable minimum surface-free energy for oriented growth along that direction (Ref 30). The diffractogram also shows many broad and less intense peaks throughout the region, which is the characteristic of nanoscale materials. The small peak at 23.14° for (020) plane in undoped films has been found to be totally suppressed with doping. The lattice parameters (a and b) somewhat decrease with the Sn doping. This decrease in the lattice parameter may be due to substitution incorporation of Sn ions into the lattice network. Also the average crystallite size has been found to decrease with Sn doping. This may be due to the increase in the density of nucleation centers at the time of film growth which, in turn, increases lattice strain of the films. The other outcome of Sn doping in the film is the shifting of the (200) peak position toward higher values of 2θ compared to the peak position in undoped film. This may be due to incorporation of Sn ions into WO_3 lattice as the ionic radii of W^{6+} and Sn^{4+} are 0.062 nm and 0.069 nm, respectively. The lattice parameters (a, b, c, and β), the crystallite size (D), and the lattice strain (ε) of the films, listed in Table 1, have been determined using the monoclinic equation (Ref 27), the Debye-Scherrer formula (Ref 27), and the tangent formula (Ref 27). The standard deviation (SD) for relative peak intensity is calculated from the equation (Ref 30):

$$\mathrm{SD} = \sqrt{\frac{\sum_{N=1}^{N} I_{hkl}^2 - \frac{\left(\sum_{N=1}^{N} I_{hkl}\right)^2}{N}}{N}}, \qquad \text{(Eq 1)}$$

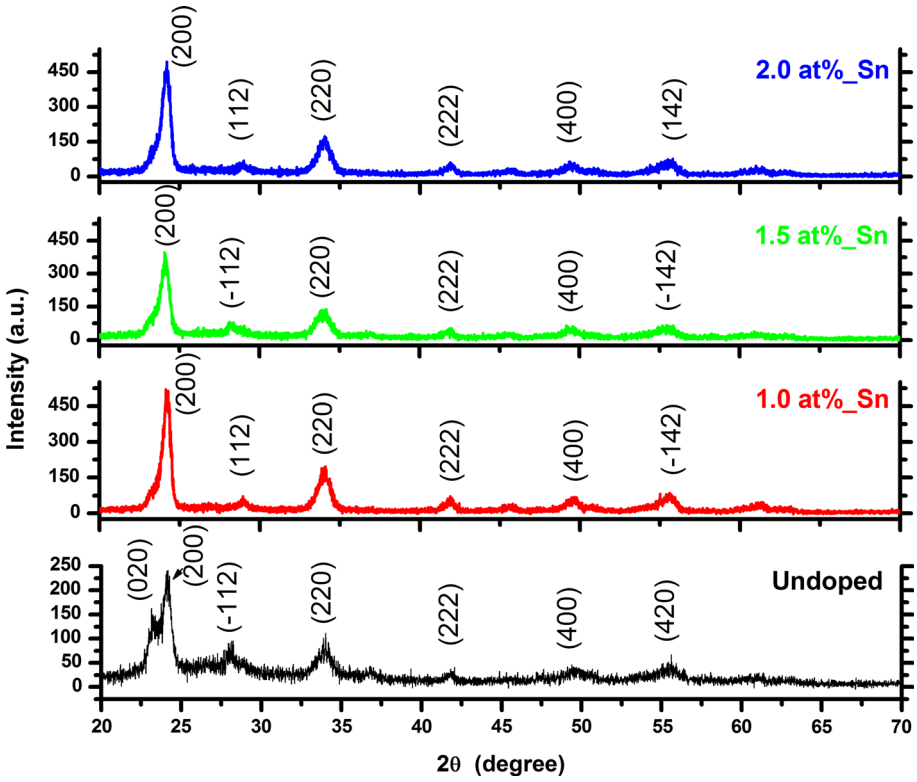

Fig. 1 XRD spectra of the undoped and Sn-doped WO_3 thin films

where I_{hkl} is the relative intensity of an (h k l) plane, and N is the number of peaks observed in the XRD spectra of the films. It has been found that SD increases with the increase of doping concentration, indicating increase in heterogeneous nucleation. The texture coefficient (TC) of the films has been determined using the equation (Ref 27). The higher value of TC in all the films indicates good textured growth. The variation of SD and TC with doping concentration is shown in Fig. 2.

3.1.2 SEM and AFM Analyses. The surface morphology using SEM images of the undoped and Sn-doped films is presented in Fig. 3. The undoped film has uniform and homogeneous surface having fine crystallites without any faulty zones on the film. On Sn doping, appearance of island-like structure (i.e., cluster of primary crystallites at few places) takes place. However, no visible holes or faulty zones over the film surface are observed in the doped films. The EDX results of the films are shown in Fig. 4 which confirms the presence of tin ions into WO_3 films. The scanned area on film for EDX is 300 μm × 300 μm, which has been chosen at different locations of film to know the uniformity of atomic distribution. The two-dimensional (2D) and three-dimensional (3D) AFM images of the undoped and Sn-doped WO_3 thin films are shown in Fig. 5(a) and (b), respectively, scanned over an area of (1 μm × 1 μm). The 3D images of the samples exhibit coalescence of grains, and the extent of coalescence begins to decrease on Sn doping. In the case of 2 at.% Sn-doped sample, large nicely separated conical columnar grains are observed throughout the surface. The average surface roughness of the films is listed in Table 1.

3.2 Optical Studies

3.2.1 UV-Visible Spectra Analyses. The knowledge of optical parameters of thin films is of great importance for successful application in optoelectronics devices. The transmittance and reflectance spectra of the undoped and doped films in the wavelength range 320-800 nm are shown in Fig. 6. The transmittance has been found to decrease in all the Sn-doped films. This is due to the fact that with Sn doping, defects, and island-like structures (as evident from SEM images) in WO_3 develop. Therefore, the incident light interacting with them gets scattered which results in low transmittance for the doped samples. Also, the transmittance in transparent metal oxides semiconductors depends on the metal to oxygen ratio. A film shows less transparency when the amount of metal increases (Ref 31).

The optical band gap has been calculated for both direct and indirect transitions, because regarding the nature of transition, some authors consider it to be direct (Ref 13, 32), while some others believe it to be indirect (Ref 28, 33), and some reported both the values (Ref 11, 26). From the absorption spectra, the optical band gap, E_g, has been determined on the basis of the well-known relation (Ref 34)

$$\alpha h\nu = K\left(h\nu - E_g\right)^p, \qquad \text{(Eq 2)}$$

Table 1 Structural parameters of WO_3 thin films

XRD Analyses													AFM analyses
WO_3 film	Position	d-Spacing observed	d-Spacing JCPDS	*hkl*	TC	Crystallite size, nm		Lattice strain, %	*a*, Å	*b*, Å	*c*, Å	β, °	Average roughness, nm
Undoped	23.144	3.840	3.769	020	0.7051	16.89	Average crystallite	0.0102	7.434	7.680	7.453	96.885	6.46
	24.098	3.690	3.648	200	1.3431	24.18	size: 13.97	0.0069					
	28.140	3.169	3.117	−112	1.8141	17.06		0.0084					
	34.033	2.632	2.621	220	0.6111	07.21		0.0164					
	36.813	2.440	2.516	122	1.4035	14.54		0.0076					
	41.788	2.160	2.154	222	0.7356	11.07		0.0088					
	49.621	1.836	1.824	400	0.5762	09.12		0.0091					
	55.922	1.643	1.642	420	0.8112	11.71		0.0063					
1.0 at.% Sn	24.312	3.658	3.648	200	1.2030	18.81	Average crystallite	0.0088	7.320	7.598	7.305	88.091	1.46
	28.950	3.082	3.083	112	0.4444	17.09	size: 13.82	0.0081					
	33.995	2.635	2.621	220	0.6984	10.82		0.0120					
	41.920	2.153	2.154	222	0.8264	12.66		0.0077					
	45.661	1.985	1.996	−312	1.2311	11.22		0.0080					
	49.724	1.832	1.824	400	0.5335	08.29		0.0099					
	55.673	1.650	1.651	−142	2.1448	15.60		0.0048					
	61.293	1.511	1.502	422	0.9183	16.03		0.0042					
1.5 at.% Sn	24.186	3.677	3.648	200	1.4620	13.02	Average crystallite	0.0127	7.400	7.601	7.462	83.587	3.89
	28.248	3.157	3.117	−112	1.2592	17.07	size: 12.17	0.0083					
	33.896	2.643	2.621	220	0.7703	10.81		0.0110					
	36.890	2.435	2.516	122	0.8675	14.54		0.0075					
	41.843	2.157	2.154	222	0.9053	11.07		0.0088					
	45.738	1.982	1.996	−312	1.2524	11.23		0.0079					
	49.410	1.843	1.824	400	0.5914	07.59		0.0109					
	61.118	1.515	1.502	422	0.8919	12.01		0.0057					
2.0 at.% Sn	24.199	3.675	3.648	200	1.5017	18.81	Average crystallite	0.0088	7.352	7.498	7.698	88.635	2.08
	28.980	3.079	3.083	112	0.4805	10.68	size: 12.46	0.0130					
	34.137	2.624	2.621	220	0.7462	09.62		0.0123					
	41.964	2.151	2.154	222	0.8929	14.77		0.0066					
	45.657	1.985	1.996	−312	1.4366	08.98		0.0099					
	49.493	1.840	1.824	400	0.5384	11.39		0.0073					
	55.776	1.647	1.642	142	1.4750	13.38		0.0055					
	61.322	1.511	1.502	422	0.9286	12.03		0.0057					

where p has discrete values like 1/2, 3/2, 2, or more depending on whether the transition is direct or indirect, and allowed or forbidden. In the direct and allowed cases, $p = ½$, whereas for direct but forbidden cases, it is 3/2. But for the indirect and allowed cases, $p = 2$, and for the forbidden cases, it will be 3 or more. K is a constant given by equation (Ref 34):

$$K = \left[e^2/\left(\pi n e m_e^* h^2\right)\right](2m_r)^{\frac{3}{2}}, \quad \text{(Eq 3)}$$

where m_e^* and m_r are the effective and reduced masses of charge carriers, respectively. E_g is the optical band gap.

The direct optical band gap (E_g) has been determined by extrapolating the linear portion of the plot $(Ahv)^2$ to the energy axis (hv), shown in Fig. 7(a). The optical band gap of undoped WO_3 thin film has been found to be 3.34 eV, which lies in between 3.65 and 3.27 eV for the amorphous and the crystalline WO_3 films, respectively, as reported by Deb (Ref 35). On Sn doping, the band gap shows a red shift and becomes 2.89 eV at 2 at.% doping. This band gap narrowing with doping is a common phenomenon in most oxide semiconductors (Ref 36, 37). It has been explained by considering that near the conduction band edge and valence band edge, the sub energy levels are created by donor and acceptor impurities. As doping percentage increases, the number of defect levels increases due to which the band edge is shifted deep into the forbidden gap, resulting in reduction in the band gap energy (Ref 38). This band gap reduction with doping is a good criterion for its application in solar cells (Ref 39).

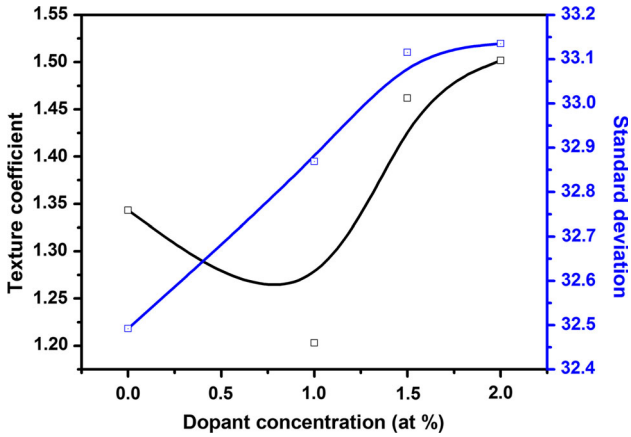

Fig. 2 Variation of texture coefficient and standard deviation with dopant concentration

Figure 7(b) shows the plot of $(Ahv)^{1/2}$ versus (hv) for indirect band gap (E_{gind}). The indirect band gap energy

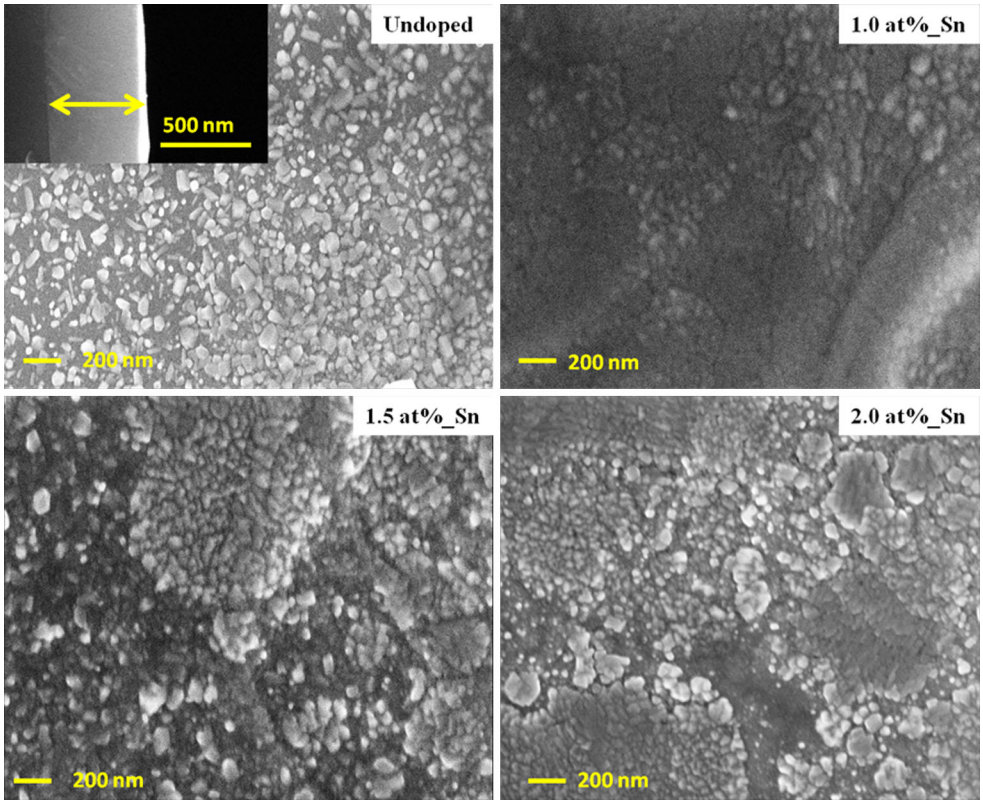

Fig. 3 SEM images of WO_3 thin films (Inset shows cross-sectional SEM image)

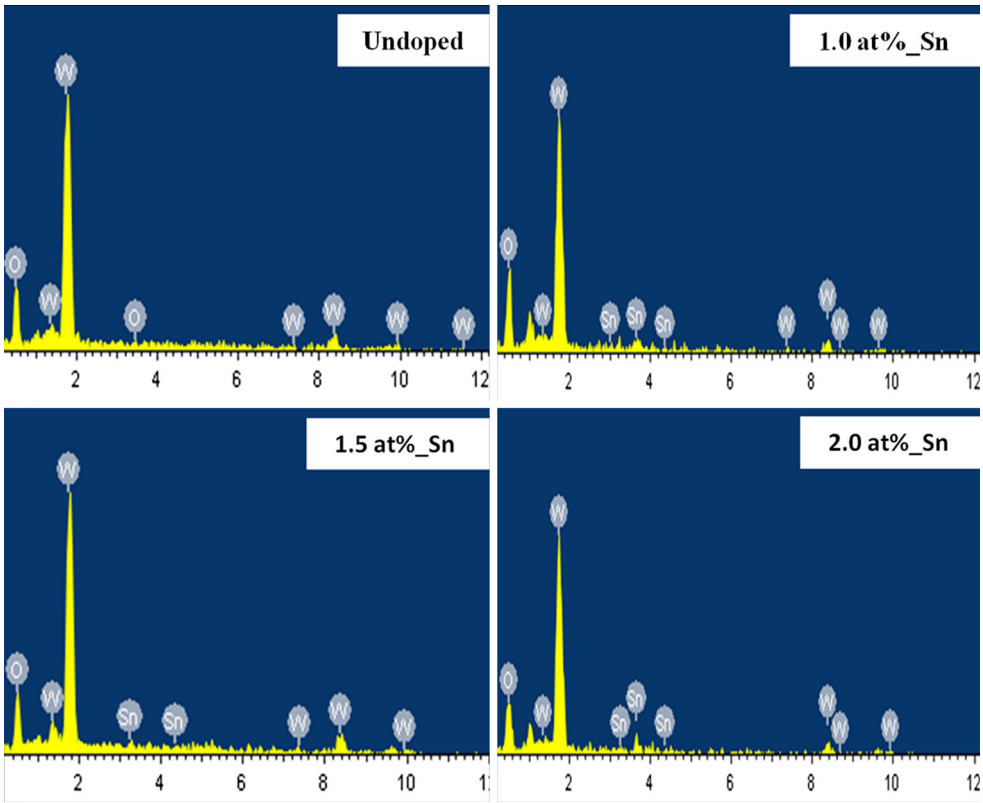

Fig. 4 EDX images of the undoped and Sn-doped WO_3 thin films

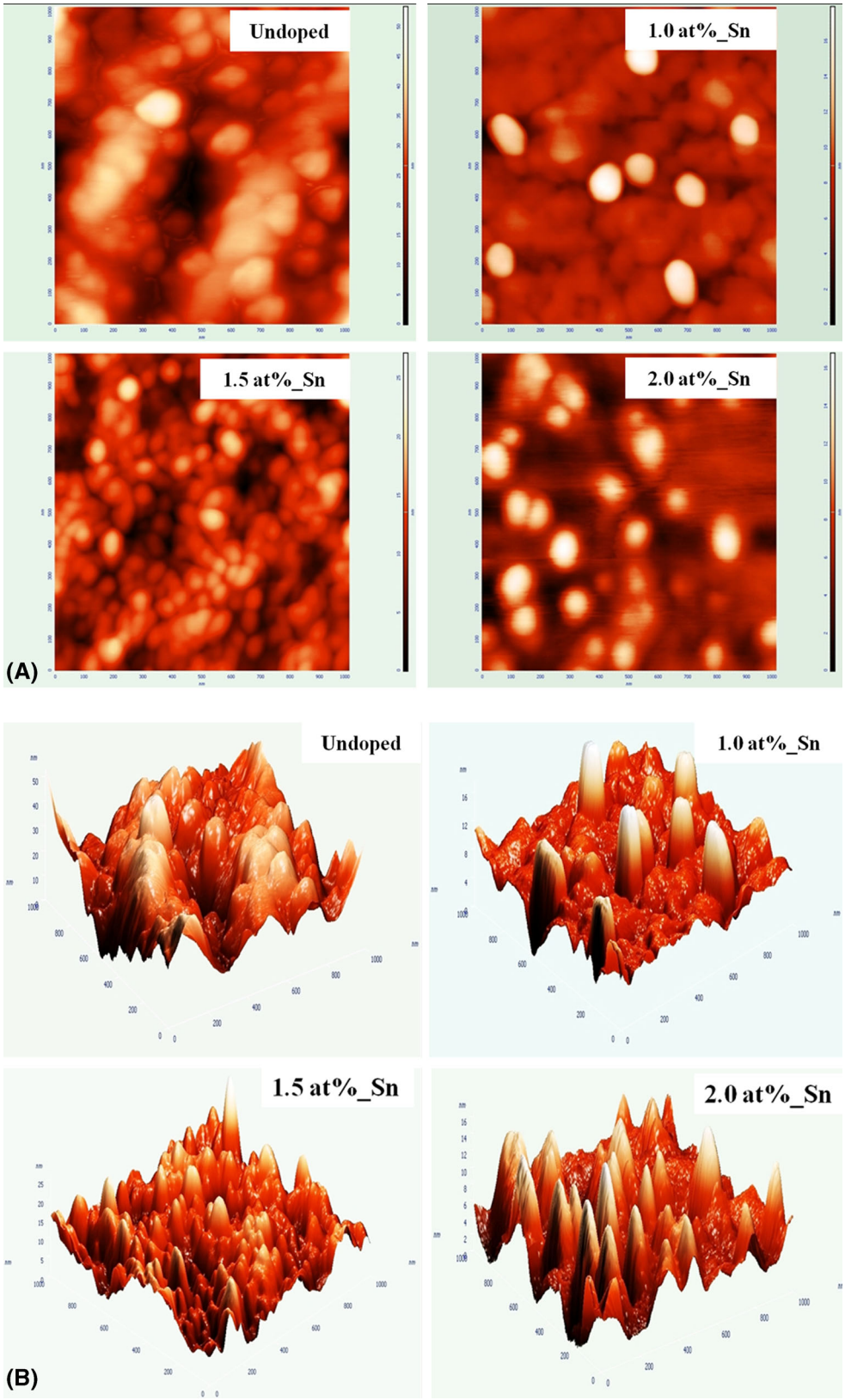

Fig. 5 (a) 2D AFM images of WO_3 thin films. (b) 3D AFM images of WO_3 thin films

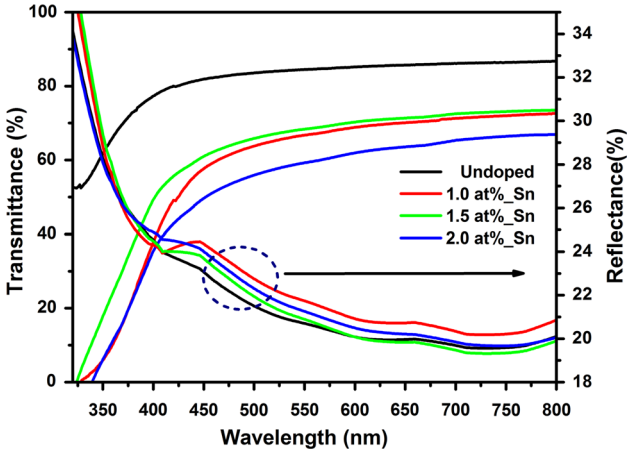

Fig. 6 Transmittance and reflectance spectra of the undoped and Sn-doped WO_3 thin films

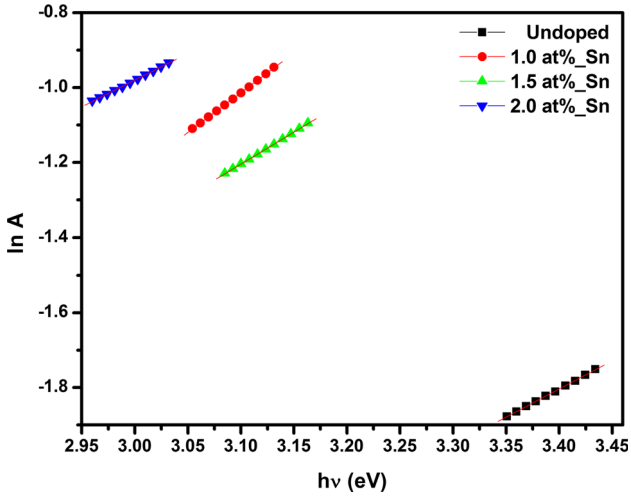

Fig. 8 Plot of lnA vs. $h\upsilon$

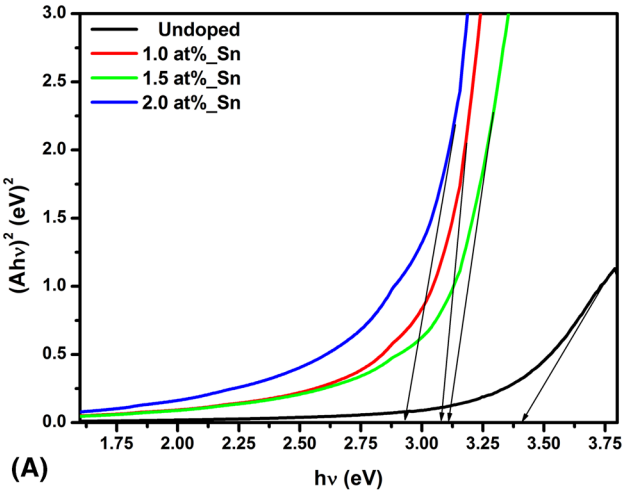

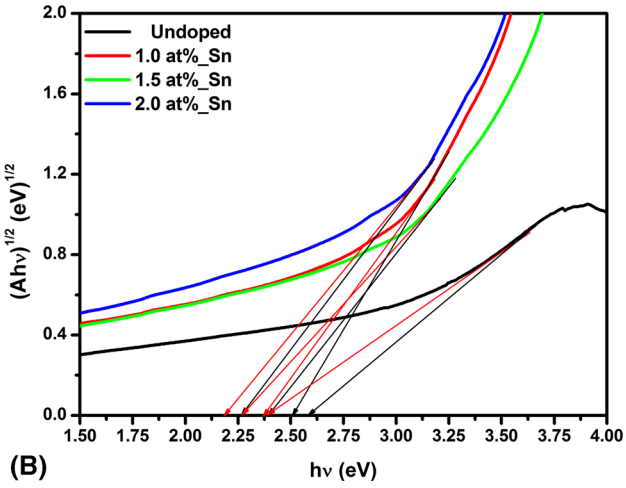

Fig. 7 (a) Plot of $(Ah\upsilon)^2$ vs. $h\upsilon$. (b) Plot of $(Ah\upsilon)^{1/2}$ vs. $h\upsilon$

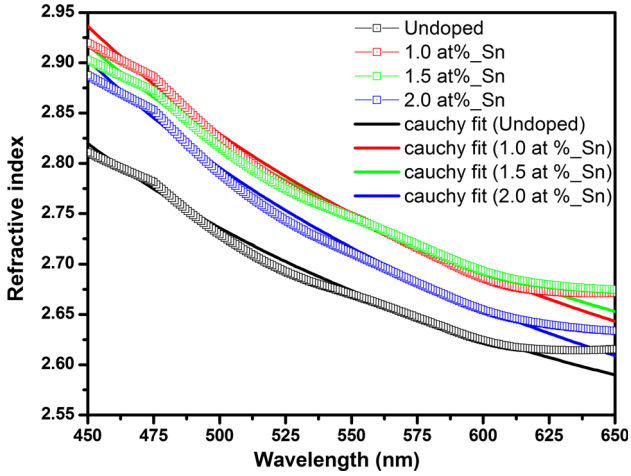

Fig. 9 Variation of refractive index and Cauchy's fit with wavelength

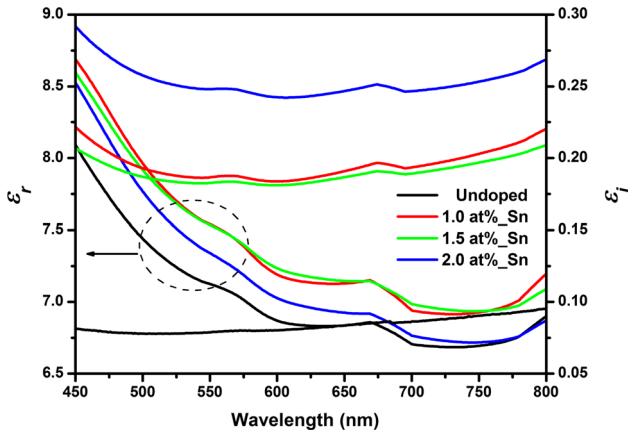

Fig. 10 Wavelength dependence of real and imaginary parts of dielectric constant of WO_3 thin films

and the phonon energy (E_p) have been calculated by resolving the plot into two distinct straight line portions. The straight line corresponding to phonon absorption process occurred at lower photon energies cuts the energy axis at ($E_{gind} - E_p$), whereas the straight line in the relatively higher energy range corresponding to phonon emission process cuts the energy axis at ($E_{gind} + E_p$) (Ref 30, 40). The values of E_{gind} for the undoped and the doped films have lower value than E_g. Also, here E_{gind} shows the red shift on doping.

It has been found that near the fundamental absorption edge, the absorption coefficient α exponentially varies on the incident photon energy and follows the well-known Urbach relation expressed as (Ref 27)

$$\alpha = \alpha_o \exp\left(\frac{h\nu}{E_o}\right), \quad \text{(Eq 4)}$$

where α_o is a constant, and E_o is Urbach energy describing the width of the localized states in the band gap. In terms of absorption, the above equation can be written as

$$A = A_o \exp\left(\frac{h\nu}{E_o}\right), \quad \text{(Eq 5)}$$

where A_o is another constant. E_o is estimated from the slope of the linear relationship $ln\ A$ versus $h\nu$, shown in Fig. 8. Spectral variation of refractive index (n) of the films in the wavelength range 450-650 nm is presented in Fig. 9. From the reflectance data, refractive index has been calculated using the relation (Ref 34):

$$n = \left(\frac{R+1}{1-R}\right) + \sqrt{\frac{4R}{(R-1)^2} - k^2}, \quad \text{(Eq 6)}$$

where R and k are reflectance and extinction coefficient, respectively. And the dispersion of the refractive index is fitted to the Cauchy's relation using the equation (Ref 34):

$$n = A' + \frac{B'}{\lambda^2}, \quad \text{(Eq 7)}$$

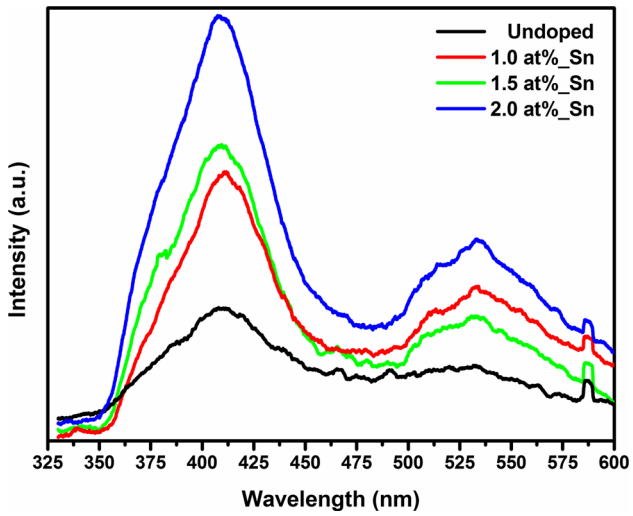

Fig. 11 Room temperature PL spectra of WO_3 thin films

where A' and B' are the Cauchy's constants, and λ is the wavelength of light. Both the undoped and doped films are found to be well fitted into the Cauchy's relation. The refractive index satisfies the relations ($2.38 + 89413.99/\lambda^2$), ($2.37 + 114057.98/\lambda^2$), ($2.41 + 102995.30/\lambda^2$), and ($2.34 + 114281.04/\lambda^2$) for the undoped, 1, 1.5, and 2 at.% doped films, respectively. Thus, all the films show normal dispersion in the wavelength range of 450-625 nm.

The complex dielectric constant is a fundamental intrinsic property of any material. The real part of the dielectric constant implies the degree of retardation in the velocity of light that passes through the material, while the imaginary part implies how a dielectric material absorbs energy from an electric field due to dipole motion. The real and the imaginary parts of the dielectric constant also provide the loss factor which is the ratio of the imaginary part to the real part of the dielectric constant (Ref 41). The complex dielectric constant ε_c is given by the relation (Ref 34):

$$\varepsilon_c = \varepsilon_r + \varepsilon_i = (n + ik)^2, \quad \text{(Eq 8)}$$

where real part ε_r is the normal dielectric constant, and imaginary part ε_i represents the absorption associated with free carriers. The spectral variation of the real and imaginary part of dielectric constant is shown in Fig. 10.

3.2.2 Photoluminescence Studies. The PL spectra of nanocrystalline tungsten oxide thin films are less investigated. Manfredi et al. (Ref 42) have reported that photoluminescence in tungsten oxide does not appear at room temperature. But in the present investigation, we have observed photoluminescence in nanocrystalline WO_3 thin films at room temperature. Figure 11 shows the room temperature PL emission spectra of undoped and doped WO_3 thin films. Two distinct peaks, one blue emission at 408 nm and other green emission at 533 nm, are observed in the PL spectra. The emission peak at 408 nm is due to the recombination of free excitons and referred to as near

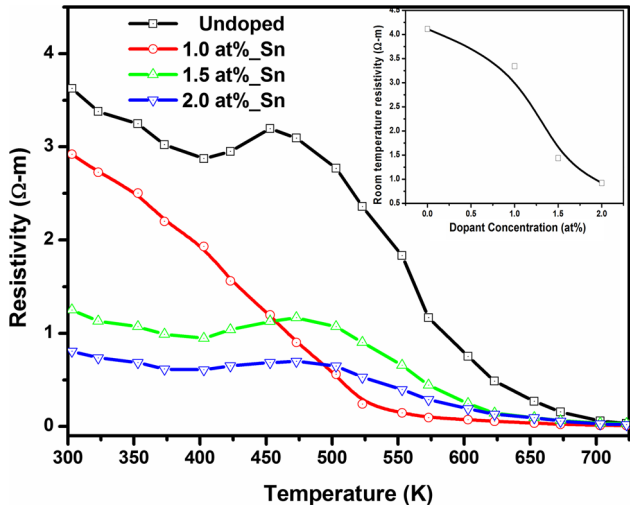

Fig. 12 Variation of electrical resistivity of the WO_3 films with temperature (inset shows room temperature resistivity as a function of dopant concentration.)

band edge emission (NBE), whereas the emission at 533 nm may be attributed to the various luminescent centers such as defect energy levels arising due to oxygen vacancies or defects in the nanostructures. Still, there exist different controversial explanations about the PL spectra, specially the green emission. According to Groenink and Blasse (Ref 43) and Korzhik and co-workers (Ref 44-46), the green emission originates from (WO_3 + F) centers. Sinelnikov et al. (Ref 47) have concluded that the WO_4 tetrahedra distorted upon the formation of oxygen vacancies are responsible for the green luminescence band. On the other hand, several authors attribute the green photoluminescence to defect centers associated with interstitial oxygen (Ref 48).

The NBE emission peak intensity in the doped films has been found to enhance relative to that of the undoped film. Density of free excitons is the major factor affecting the intensity of NBE emission (Ref 49). We observe a variation in intensity throughout the spectrum with varying Sn content.

3.3 Electrical Studies

The knowledge of electrical conductivity of WO_3 thin films is important and essential for making successful practical devices. Hence a detail study of electrical behavior of undoped and Sn-doped films has been carried out through resistance versus temperature measurements.

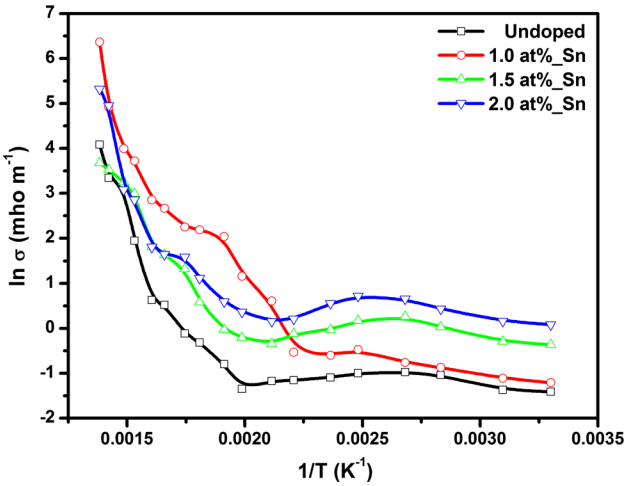

Fig. 13 Plot of $ln\sigma$ with $1/T$

In the present investigation, the room temperature electrical resistivity of undoped WO_3 thin films has been found to be 4.11 Ω-m which decreases significantly on Sn doping (shown in inset of Fig. 12). Decrease in resistivity with Sn dopant concentration may be attributed to incorporation of tin ions into WO_3 lattice, resulting in increase in oxygen vacancy/carrier concentration. Also, based on the size effects of electrical conductivity, when the crystallite size is below ~25 nm, the grain boundary scattering decreases significantly and therefore increases the conductivity (Ref 50). Lethy et al. (Ref 39) have reported room temperature electrical resistivity of laser ablated nanostructured pure WO_3 thin film to be 17 Ω m, which increases with increase in titania content up to 5 wt.%, and on further doping to 10 wt.%, the resistivity decreases significantly. Whilst Patil et al. (Ref 51) have reported decrease in room temperature electrical resistivity of spray-deposited WO_3 thin films on TiO_2 doping. Authors have studied the effect of In doping on the electrical conductivity of spray-deposited WO_3 thin films prepared using WCl_6 dissolved in *N-N* dimethylformamide and found the room temperature conductivity increases on In doping (Ref 27).

Temperature dependence of electrical resistivity of WO_3 thin films in the temperature range 303-723 K is shown in Fig. 12. The decrease in resistivity with temperature indicates the semiconductor behavior of the films. In fact, resistivity is the result of trade-off between two competing processes occurring simultaneously, namely, thermal excitation of electrons and adsorption of atmospheric oxygen on the film surface.

The electronic transport of WO_3, in general, is believed to be controlled by the hopping conduction process, and the electrons are the major carriers via the oxygen vacancies (Ref 52). The electrical conductivity σ can be expressed as

$$\sigma = \sigma_o \exp\left(\frac{-E_a}{k_B T}\right), \qquad \text{(Eq 9)}$$

where E_a and k_B are the activation energy and Boltzman constant, respectively. The activation energies are obtained from the slope of plot showing ln σ versus $1/T$ (Fig. 13) and are listed in Table 2. All the films exhibit two activation energies in different temperature regions. The results indicate the presence of two defect energy levels—one deep and one shallow near the bottom of the conduction band.

Table 2 Optical and electrical parameters of undoped and Sn-doped WO_3 thin films

WO_3 film	Direct band gap E_g, eV	Indirect band gap E_{gind}, eV	Phonon energy E_p, meV	Urbach energy E_o, meV	Reflective index n at 550 nm	Activation energy at temperature range E_a, eV		Room temperature resistivity ρ, Ω-m
						303-403 K	523-723 K	
Undoped	3.34	2.62	98.50	665.91	2.6149	0.0526	0.7635	4.1125
1.0 at.%_Sn	3.04	2.53	65.00	469.50	2.7437	0.0757	0.5992	3.3425
1.5 at.%_Sn	3.07	2.43	60.00	584.99	2.7444	0.0690	0.6021	1.4408
2.0 at.%_Sn	2.89	2.34	35.00	704.08	2.7090	0.0741	0.6635	0.9217

4. Conclusion

Undoped WO_3 and Sn-doped thin films were prepared using chemical spray pyrolysis, with dopant concentration (Sn/W ratio) varying from 0 to 2 atomic percent (at.%). XRD analyses confirm the monoclinic phase of the prepared films with the highest intensity along (200) direction for all the samples. The average crystallite size has been found to decrease with Sn doping. EDX results confirm the presence of tin ions into WO_3 films. The 3D AFM images of the films exhibit coalescence of grains, and the extent of coalescence begins to decrease on Sn doping. The UV-visible spectroscopy studies show a direct optical band gap of 3.34 eV and an indirect band gap of 2.62 eV in the undoped film. From the reflectance data, refractive index has been calculated, and all the films exhibit normal dispersion in the wavelength range of 450-625 nm. PL spectra shows enhancement in intensity throughout the spectrum with the increase of Sn content. The films exhibit two activation energies in different temperature regions, corresponding to two defect energy levels.

Acknowledgments

The authors are grateful to Dr. E. Mohandas, Head, Materials Synthesis and Structural Characterization Division, Indira Gandhi Centre for Atomic Research (IGCAR), Kalpakkam India, for providing XRD facilities. They would wish to further express their gratitude to the Head, Institute Instrumentation Centre, Indian Institute of Technology, Roorkee, India for providing SEM and AFM measurement facilities. Kind support extended by Mr. Saikat Chakraborty, Department of Physics, Banaras Hindu University, Varanasi, India is also acknowledged. Financial support provided by the University Grants Commission, New Delhi, India, in the form of a major research project (No. 40-450/2011 (SR)) is gratefully acknowledged.

References

1. C.G. Granqvist, Electrochromic Tungsten Oxide Films: Review of Progress 1993-1998, *Sol. Energy Mater. Sol. Cells*, 2000, **60**, p 201-262
2. A. Romanyuk and P. Oelhafen, Evidence of Different Oxygen States During Thermal Coloration of Tungsten Oxide, *Sol. Energy Mater. Sol. Cells*, 2006, **90**, p 1945-1950
3. C.S. Blackman and I.P. Parkin, Atmospheric Pressure Chemical Vapor Deposition of Crystalline Monoclinic WO_3 and WO_{3-x} Thin Films from Reaction of WCl_6 with O-Containing Solvents and their Photochromic and Electrochromic Properties, *Chem. Mater.*, 2005, **17**, p 1583-1590
4. M. Ranjbar, S. Fardindoost, S.M. Mahdavi, A.I. Zad, and N. Tahmasebi, Palladium Nanoparticles Deposition onto the WO_3 Surface Through Hydrogen Reduction of PdCl2: Characterization and Gasochromic Properties, *Sol. Energy Mater. Sol. Cells*, 2011, **95**, p 2335-2340
5. M. Penza, M.A. Tagliente, L. Mirenghi, C. Gerardi, C. Martucci, and G. Cassano, Tungsten Trioxide (WO_3) Sputtered Thin Films for a NO_x Gas Sensor, *Sens. Actuators B*, 1998, **50**, p 9-18
6. N. Muthuraman, P.K. Guruvaiah, and P.G. Agneeswara, High Performance Carbon Supported Pt-WO_3 Nanocomposite Electrocatalysts for Polymer Electrolyte Membrane Fuel Cell, *Mater. Chem. Phys.*, 2012, **133**, p 924-931
7. R. Azimirad, N. Naseri, O. Akhavan, and A.Z. Moshfegh, Hydrophilicity Variation of WO_3 Thin Films with Annealing Temperature, *J. Phys. D Appl. Phys.*, 2007, **40**, p 1134
8. N. Naseri, R. Azimirad, O. Akhavan, and A.Z. Moshfegh, The Effect of Nanocrystalline Tungsten Oxide Concentration on Surface Properties of Dip-Coated Hydrophilic WO_3-SiO_2 Thin Films, *J. Phys. D Appl. Phys.*, 2007, **40**, p 2089
9. K.M. Karuppasamy and A. Subrahmanyam, The Electrochromic and Photocatalytic Properties of Electron Beam Evaporated Vanadium-Doped Tungsten Oxide Thin Films, *Sol. Energy Mater. Sol. Cells*, 2008, **92**, p 1322-1326
10. M. Feng, A.L. Pan, H.R. Zhang, Z.A. Li, F. Liu, H.W. Liu, D.X. Shi, B.S. Zou, and H.J. Gao, Strong Photoluminescence of Nanostructured Crystalline Tungsten Oxide Thin Films, *Appl. Phys. Lett.*, 2005, **86**, p 141901-141903
11. M. Kovendhan, D.P. Joseph, E.S. Kumar, A. Sendilkumar, P. Manimuthu, S. Sambasivam, C. Venkateswaran, and R. Mohan, Structural Transition and Blue Emission in Textured and Highly Transparent Spray Deposited Li Doped WO_3 Thin Films, *Appl. Surf. Sci.*, 2011, **257**, p 8127-8133
12. X. He, J. Li, X. Gao, and L. Wang, NO_2 Sensing Characteristics of WO_3 Thin Film Micro Gas Sensor, *Sens. Actuators B*, 2003, **93**, p 463-467
13. S. Dabbous, T.B. Nasrallah, J. Ouerfelli, K. Boubaker, M. Amlouk, and S. Belgacem, Study of Structural and Optical Properties of Sprayed WO_3 Thin Films Using Enhanced Characterization Techniques Along with the Boubaker Polynomials Expansion Scheme (BPES), *J. Alloys Compd.*, 2009, **487**, p 286-292
14. A. Karuppasamy and A. Subrahmanyam, Studies on Electrochromic Smart Windows Based on Titanium Doped WO_3 Thin Films, *Thin Solid Films*, 2007, **516**, p 175-178
15. A.H. Jayatissa, S.T. Cheng, and T. Gupta, Annealing Effect on the Formation of Nanocrystals in Thermally Evaporated Tungsten Oxide Thin Films, *Mater. Sci. Eng. B*, 2004, **109**, p 269-275
16. C.H. Hsu, C.C. Chang, C.M. Tseng, C.C. Chan, W.H. Chao, Y.R. Wu, M.H. Wen, Y.T. Hsieh, Y.C. Wang, C.L. Chen, M.J. Wang, and M.K. Wu, An Ultra-Fast Response Gasochromic Device for Hydrogen Gas Detection, *Sens. Actuators B*, 2013, **186**, p 193-198
17. M.H. Yaacob, M.Z. Ahmad, A.Z. Sadek, J.Z. Ou, J. Campbell, K.K. Zadeh, and W. Wlodarski, Optical Response of WO_3 Nanostructured Thin Films Sputtered on Different Transparent Substrates Towards Hydrogen of Low Concentration, *Sens. Actuators B*, 2013, **177**, p 981-988
18. T. Tesfamichael, A. Ponzoni, M. Ahsan, and G. Faglia, Gas Sensing Characteristics of Fe-Doped Tungsten Oxide Thin Films, *Sens. Actuators B*, 2012, **168**, p 345-353
19. C.W. Lai and S. Sreekantan, Fabrication of WO_3 Nano Structures by Anodization Method for Visible-Light Driven Water Splitting and Photodegradation of Methylorange, *Mater. Sci. Semicond. Process.*, 2013, **16**, p 303-310
20. M. Deepa, P. Singh, S.N. Sharma, and S.A. Agnihotry, Effect of Humidity on Structure and Electrochromic Properties of sol-Gel-Derived Tungsten Oxide Films, *Sol. Energy Mater. Sol. Cells*, 2006, **90**, p 2665-2682
21. S.K. Biswas and J.O. Baeg, A Facile One-Step Synthesis of Single Crystalline Hierarchical WO_3 with Enhanced Activity for Photoelectrochemical Solar Water Oxidation, *Int. J. Hydrog. Energy*, 2013, **38**, p 3177-3188
22. C.O. Avellaneda, P.R. Bueno, R.C. Faria, and L.O.S. Bulhoes, Electrochromic Properties of Lithium Doped WO_3 Films Prepared by the Sol-Gel Process, *Electrochim. Acta*, 2001, **46**, p 1977-1981
23. R. Mukherjee, C.S. Prajapati, and P.P. Sahay, Tailoring the Microstructural, Optical and Electrical Properties of Nanocrystalline WO_3 Thin Films Using Al Doping, *J. Mater. Eng. Perform.*, 2014, doi:10.1007/s11665-014-1094-5
24. K.W. Park, Electrochromic Properties of Au-WO_3 Nanocomposite Thin-Film Electrode, *Electrochim. Acta*, 2005, **50**, p 4690-4693

25. S.R. Bathe and P.S. Patil, Titanium Doping Effects in Electrochromic Pulsed Spray Pyrolysed WO_3 Thin Films, *Solid State Ion.*, 2008, **179**, p 314-323
26. J. Gaury, E.M. Kelder, E. Bychkov, and G. Biskos, Characterization of Nb-Doped WO_3 Thin Films Produced by Electrostatic Spray Deposition, *Thin Solid Films*, 2013, **534**, p 32-39
27. R. Mukherjee, A. Kushwaha, and P.P. Sahay, Spray-Deposited Nanocrystalline WO_3 Thin Films Prepared Using Tungsten Hexachloride Dissolved in *N-N* Dimethylformamide and Influence of In Doping on Their Structural, Optical and Electrical Properties, *Electron. Mater. Lett.*, 2014, **10**, p 401-410
28. R. Sivakumar, A.M.E. Raj, B. Subramanian, M. Jayachandran, D.C. Trivedi, and C. Sanjeeviraja, Preparation and Characterization of Spray Deposited *n*-type WO_3 Thin Films for Electrochromic Devices, *Mater. Res. Bull.*, 2004, **39**, p 1479-1489
29. K.H. Yoon, J.W. Lee, Y.S. Cho, and D.H. Kang, Structural and Photocurrent-Voltage Characteristics of Tungsten Oxide Thin Films on *p*-GaAs, *Appl. Phys. Lett.*, 1996, **68**, p 572-574
30. D.P. Joseph, M. Saravanan, B. Muthuraaman, P. Renugambal, S. Sambasivam, S.P. Raja, P. Maruthamuthu, and C. Venkateswaran, Spray Deposition and Characterization of Nanostructured Li Doped NiO Thin Films for Application in Dye-Sensitized Solar Cells, *Nanotechnology*, 2008, **19**, p 485707
31. S.S. Shinde, P.S. Shinde, Y.W. Oh, D. Haranath, C.H. Bhosale, and K.Y. Rajpure, Structural, Optoelectronic, Luminescence and Thermal Properties of Ga-Doped Zinc Oxide Thin Films, *Appl. Surf. Sci.*, 2012, **258**, p 9969-9976
32. S.R. Bathe and P.S. Patil, Electrochromic Characteristics of Fibrous Reticulated WO_3 Thin Films Prepared by Pulsed Spray Pyrolysis Technique, *Sol. Energy Mater. Sol. Cells*, 2007, **91**, p 1097-1101
33. H. Yang, F. Shang, L. Gao, and H. Han, Structure, Electrochromic and Optical Properties of WO_3 Film Prepared by Dip Coating-Pyrolysis, *Appl. Surf. Sci.*, 2007, **253**, p 5553-5557
34. A. Goswami, *Thin Film Fundamentals*, New Age International, New Delhi, 2005
35. S.K. Deb, Optical and Photoelectric Properties and Colour Centres in Thin Films of Tungsten Oxide, *Philos. Mag.*, 1973, **27**, p 801
36. X. Ding, D. Zeng, S. Zhang, and C. Xie, C-Doped WO_3 Microtubes Assembled by Nanoparticles with Ultrahigh Sensitivity to Toluene at Low Operating Temperature, *Sens. Actuators B*, 2011, **155**, p 86-92
37. N. Naseri, R. Azimirad, O. Akhavan, and A.Z. Moshfegh, Improved Electrochromical Properties of sol-gel WO_3 Thin Films by Doping Gold Nanocrystals, *Thin Solid Films*, 2010, **518**, p 2250-2257
38. B. Choudhury, M. Dey, and A. Choudhury, Defect Generation, d-d Transition, and Band Gap Reduction in Cu-Doped TiO_2 Nanoparticles, *Int. Nano Lett.*, 2013, **3**, p 25
39. K.J. Lethy, D. Beena, V.P.M. Pillai, and V. Ganesan, Bandgap Renormalization in Titania Modified Nanostructured Tungsten Oxide Thin Films Prepared by Pulsed Laser Deposition Technique for Solar Cell Applications, *J. Appl. Phys.*, 2008, **104**, p 033515
40. H. Kamal, E.K. Elmaghraby, S.A. Ali, and K.A. Hady, Characterization of Nickel Oxide Films Deposited at Different Substrate Temperatures Using Spray Pyrolysis, *J. Cryst. Growth*, 2004, **262**, p 424-434
41. N.A. Bakr, A.M. Funde, V.S. Waman, M.M. Kamble, R.R. Hawaldar, D.P. Amalnerkar, S.W. Gosavi, and S.R. Jadkar, Determination of the Optical Parameters of a-Si: H Thin Films Deposited by Hot Wire Chemical Vapour Deposition Technique Using Transmission Spectrum Only, *Pramana J. Phys.*, 2011, **3**, p 519-531
42. M. Manfredi, C. Paracchini, G.C. Salviati, and G. Schianchi, Conductive Processes in Transparent WO_3 Films Irradiated with Ultraviolet Light, *Thin Solid Films*, 1981, **79**, p 161-166
43. J.A. Groenink and G. Blasse, Some New Observations on the Luminescence of $PbMoO_4$ and $PbWO_4$, *J. Solid State Chem.*, 1980, **32**, p 9-20
44. A.A. Annenkov, M.V. Korzhik, and P. Lecoq, Lead Tungstate Scintillation Material, *Nucl. Instrum. Methods A*, 2002, **490**, p 30-50
45. P. Lecoq, I. Dafinei, E. Auffray, M. Schneegans, M.V. Korzhik, O.V. Missevitch, V.B. Pavlenko, A.A. Fedorov, A.N. Annenkov, V.L. Kostylev, and V.D. Ligun, Lead Tungstate ($PbWO_4$) Scintillators for LHC EM Calorimetry, *Nucl. Instrum. Methods A*, 1995, **365**, p 291-298
46. M.V. Korzhik, V.B. Pavlenko, T.N. Timoschenko, V.A. Katchanov, A.V. Singovskii, A.N. Annenkov, V.A. Ligun, I.M. Solskii, and J.P. Peigneux, Spectroscopy and Origin of Radiation Centers and Scintillation in $PbWO_4$ Single Crystals, *Phys. Status Solid A*, 1996, **154**, p 779-788
47. B.M. Sinelnikov, E.V. Sokolenko, and V.Y. Zvekov, The Nature of Green Luminescence Centers in Scheelite, *Inorg. Mater.*, 1996, **32**, p 999-1001
48. E. Orhan, M.A. Santos, M.A.M.A. Maurera, F.M. Pontes, C.O.P. Santos, A.G. Souza, J.A. Varela, P.S. Pizani, and E. Longo, Conditions Giving Rise to Intense Visible Room Temperature Photoluminescence in $SrWO_4$ Thin Films: The Role of Disorder, *Chem. Phys.*, 2005, **312**, p 1-9
49. C.S. Prajapati, A. Kushwaha, and P.P. Sahay, Influence of Fe Doping on the Structural, Optical and Acetone Sensing Properties of Sprayed ZnO Thin Films, *Mater. Res. Bull.*, 2013, **48**, p 2687-2695
50. D.V. Fedorov, P. Zahn, and I. Mertig, Size Effects and Conductivity of Ultrathin Cu Films, *Thin Solid Films*, 2005, **473**, p 346-350
51. P.S. Patil, S.H. Mujawar, A.I. Inamdar, P.S. Shinde, H.P. Deshmukh, and S.B. Sadale, Structural, Electrical and Optical Properties of TiO_2 Doped WO_3 Thin Films, *Appl. Surf. Sci.*, 2005, **252**, p 1643-1650
52. P. Kofstad, *Nonstoichiometry, Diffusion, and Electrical Conductivity in Binary Metal Oxides*, Wiley, New York, 1972, p 20